Acta Crystallographica Section D
Biological Crystallography
ISSN 0907-4449

The structure of augmenter of liver regeneration crystallized in the presence of 50 m*M* $CdCl_2$ reveals a novel $Cd_2Cl_4O_6$ cluster that aids in crystal packing

Quentin Florence,[a]‡ Chia-Kuei Wu,[a,b]‡ Jeffrey Habel,[a,c] J. Tucker Swindell II,[a] Bi-Cheng Wang[a] and John P. Rose[a]*

[a]Department of Biochemistry and Molecular Biology, University of Georgia, Athens, GA 30602, USA, [b]Science Applications International Corporation, McLean, VA 22102, USA, and [c]Bio-Rad Laboratories, Hercules, CA 94547, USA

‡ These authors contributed equally to this work.

Correspondence e-mail: jprose@uga.edu

Received 6 December 2011
Accepted 17 May 2012

PDB Reference: augmenter of liver regeneration, 3r7c.

The crystal structure of the protein augmenter of liver regeneration containing a 14-residue hexahistidine purification tag (hsALR) has been determined to 2.4 Å resolution by Cd-SAD using a highly redundant data set collected on a rotating-anode home X-ray source and processed in 1998. The hsALR crystal structure is a tetramer composed of two homodimers bridged by a novel $Cd_2Cl_4O_6$ cluster *via* binding to the side-chain carboxylate groups of two solvent-exposed aspartic acid residues. A comparison with the native sALR tetramer shows that the cluster dramatically changes the hsALR dimer–dimer interface, which can now better accommodate the extra 14 N-terminal residues associated with the purification tag. The refined 2.4 Å resolution structure is in good agreement with both the X-ray data (R_{cryst} of 0.165, R_{free} of 0.211) and the expected stereochemistry (r.m.s. deviations from ideality for bond lengths and bond angles of 0.007 Å and 1.15°, respectively).

1. Introduction

Augmenter of liver regeneration (ALR) is an FAD-containing protein that was first isolated in the cytosol from regenerating rat liver and was found to augment the rate of liver regeneration in the presence of other factors (Francavilla *et al.*, 1987). Since then, studies have associated ALR with immunosuppression (Francavilla *et al.*, 1997; Tanigawa *et al.*, 2000), enhancement of pancreatic transplantation (Adams *et al.*, 1998), mitochondrial gene expression (Polimeno *et al.*, 2000), the export of iron–sulfur (Fe–S) clusters (Lange *et al.*, 2001) and mitochondrial intermembrane space (IMS) transport (Lisowsky *et al.*, 2001; Allen *et al.*, 2005; Lisowsky, 1996). In IMS transport, ALR has been shown to act as an FAD-linked sulfhydryl oxidase (EC 1.8.3.2) involved in the electron shuttle from Mia40 (Gerhold *et al.*, 2011; Banci *et al.*, 2011) to cytochrome *c* (Farrell & Thorpe, 2005).

In 2000, we reported the preliminary X-ray characterization of sALR containing a 14-residue (MGGSHHHHHHGMAS) N-terminal purification tag (hsALR) that unlike the native protein required the presence of 30–50 m*M* $CdCl_2$ for crystallization (Wu *et al.*, 2000). However, our initial Cd-SAD phasing attempts failed and the project was abandoned a short time later when the sALR structure was determined by the MAD method using selenomethione-labeled protein (Wu *et al.*, 2003). The hsALR crystal structure was recently revisited as a part of ongoing small-angle X-ray scattering studies of ALR–cytochrome *c* electron transport in the IMS. Here, we report the 2.4 Å resolution structure of hsALR determined by

Cd-SAD using *PHENIX* (Adams *et al.*, 2010) and the data set collected in 1998. The structure revealed a novel $Cd_2Cl_4O_6$ cluster that introduces a new mode of crystal packing which can better accommodate the 14-residue purification tag.

2. Materials and methods

2.1. Protein production, crystallization and data collection

Details of the preparation, crystallization and data-collection protocols used in this study have been reported previously (Wu *et al.*, 2000).

2.2. Structure determination and refinement

PHENIX (Adams *et al.*, 2010) aided by *Coot* (Emsley & Cowtan, 2004) was used to solve and refine the structure. Experimental phase restraints and a 4.98% R_{free} test set (Brünger, 1992) generated by *PHENIX* were used during all stages of refinement.

The *PHENIX AutoSolve* workflow was used to locate and refine positions for the anomalous scatterers, to generate and refine protein phases and to provide an initial chain trace. The FAD (flavin adenine dinucleotide) cofactor was manually fitted into the electron-density map and the model (two 80% complete hsALR dimers denoted *AC* and *BD* based on chain ID) was automatically rebuilt and refined using *AutoBuild*. Three CdX_5 moieties located on the protein surface and a Cd_2X_{10} moiety at the dimer–dimer interface were identified from $2F_o - F_c$ Fourier maps. The identity of the cadmium ligands was determined by Bijvoet difference Fourier analysis, occupancy refinement and binding geometry. A TLS model (19 TLS groups) was generated and included in the final rounds of refinement. The refinement converged to give an R_{cryst} of 0.165 and an R_{free} of 0.211, with r.m.s. deviations from ideality of 0.007 Å for bond lengths and 1.15° for bond angles. The final refined 2.4 Å resolution model is a tetramer with each monomer containing residues 14–124 plus a bound FAD. The model also contains a $Cd_2Cl_4O_6$ cluster (Fig. 1), two CdO_5 clusters, a CdO_6 cluster, six chloride ions, two sulfate ions and 237 solvent molecules modeled as waters. The 14-residue purification tag and residues 1–13 of the protein were not observed in electron-density maps, which suggests that they are disordered. Coordinates and structure factors have been deposited in the Protein Data Bank (Berman *et al.*, 2002) as entry 3r7c. Data-collection and refinement details are summarized in Table 1.

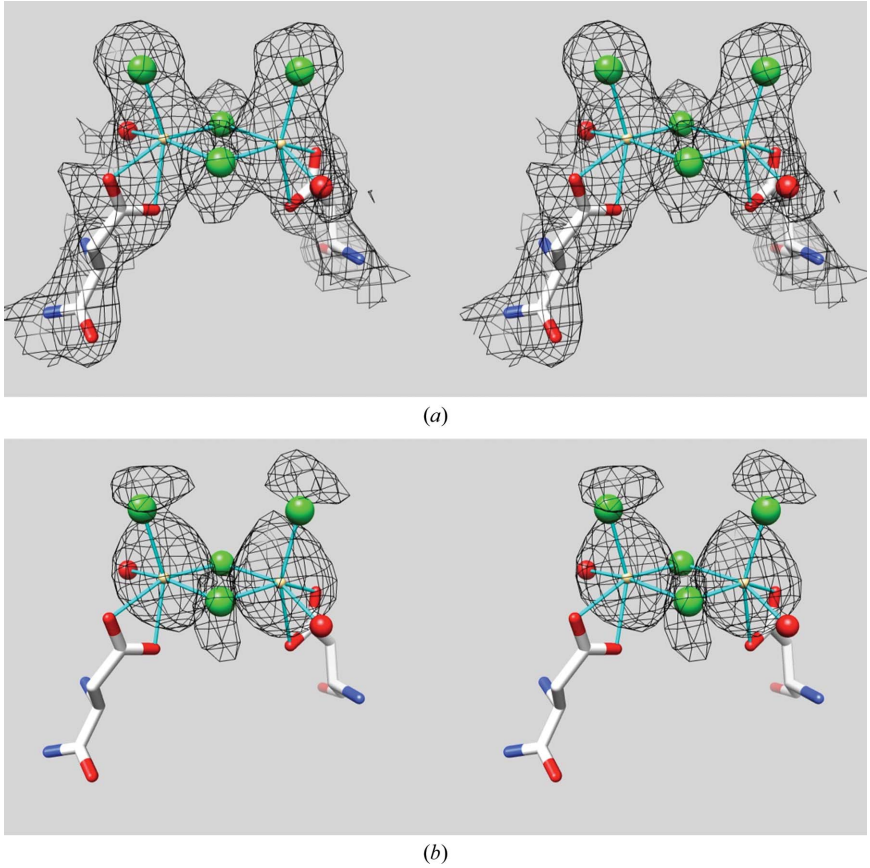

(*a*)

(*b*)

Figure 1
A cross-eyed stereoscopic view of the hsALR electron-density map centered on the Cd_2X_{10} cluster. (*a*) A $2F_o - F_c$ difference Fourier map generated using *PHENIX* and contoured at 1σ showing the quality of the Cd-SAD phases. The refined coordinates for the atoms comprising the $Cd_2Cl_4O_6$ cluster are also shown. (*b*) The Bijvoet difference Fourier map generated using *PHENIX* and contoured at 3σ used in assigning atom types and positions in the $Cd_2Cl_4O_6$ cluster. The map clearly shows the anomalous scattering density associated with the two cadmium sites and the four chloride ligands that form the cluster. Unless otherwise stated, all images were generated by *CHIMERA* (Pettersen *et al.*, 2004).

3. Results and discussion

As noted previously, initial attempts at Cd-SAD phasing in 1998 were unsuccessful. Molecular replacement (MR) using *AMoRe* (Navaza, 2001) was also explored using the native sALR *AC* dimer (PDB entry 1oqc; Rose *et al.*, 1999) as the search model. The MR analysis yielded a promising solution but the structure did not refine well, suggesting that model bias might be a problem. Since a SAD-phased structure would not suffer from model bias, the Cd-SAD study was revisited.

3.1. The hsALR structure

The hsALR structure is, as expected, very similar to the previously reported native sALR structure (PDB entry 1oqc). A *CHIMERA Match* superposition of the two structures (16 chain pairs) gives an average r.m.s. deviation (C^{α}) of 1.35 Å for chains *A*, *B* and *D* (Pettersen *et al.*, 2004). The best agreement is observed between chain *C* of hsALR and chain *A* of sALR, with an average r.m.s. deviation of 0.45 Å. The major structural differences between the native and His-tagged structures (see Fig. 2*c*) are centered on the loop spanning residues

60–68 which forms the mouth of the FAD-binding pocket and contains the active-site residues Cys62 and Cys65. For chains *A*, *B* and *D* a long loop connecting α2 and α3 (residues 68–76) is observed. Chain *C*, however, exhibits a much shorter loop (residues 60–63) and helix α3 lengthens to span residues 62–76, closely resembling the loop observed in the native sALR structure. The hsALR monomers also exhibit structural variability, with r.m.s. deviations on superposition ranging from 0.37 Å (on superimposing chains *A* and *B*) to 1.37 Å (on superimposing chains *A* and *C*). Again, the loop connecting helices α2 and α3 shows the most variation. The interaction of Asp74 with the $Cd_2Cl_4O_6$ cluster appears to stabilize the α2–α3 loop in the *A* and *B* monomers, as reflected by their close structural similarity. Superposition of the four monomers in the native structure shows less structural variability, giving an average C^{α} r.m.s. deviation (six chain pairs) of 0.292 Å and may explain our problems associated with model bias in the MR structure determination.

The conformational variability observed in this region can in part be attributed to the presence of the $Cd_2Cl_4O_6$ cluster, which is anchored to chains *A* and *B* by Asp74 as described below. The plasticity of this region is also reflected by the increased temperature factors found for residues in this loop and may be a further indicator of the dynamics of the ALR catalytic site needed to accommodate Mia40, its potential redox partner.

3.2. The $Cd_2Cl_4O_6$ cluster

The key feature of the hsALR structure is the novel $Cd_2Cl_4O_6$ cluster (Fig. 3*a*) found at the dimer–dimer interface of the hsALR tetramer. Cadmium cations have been shown to

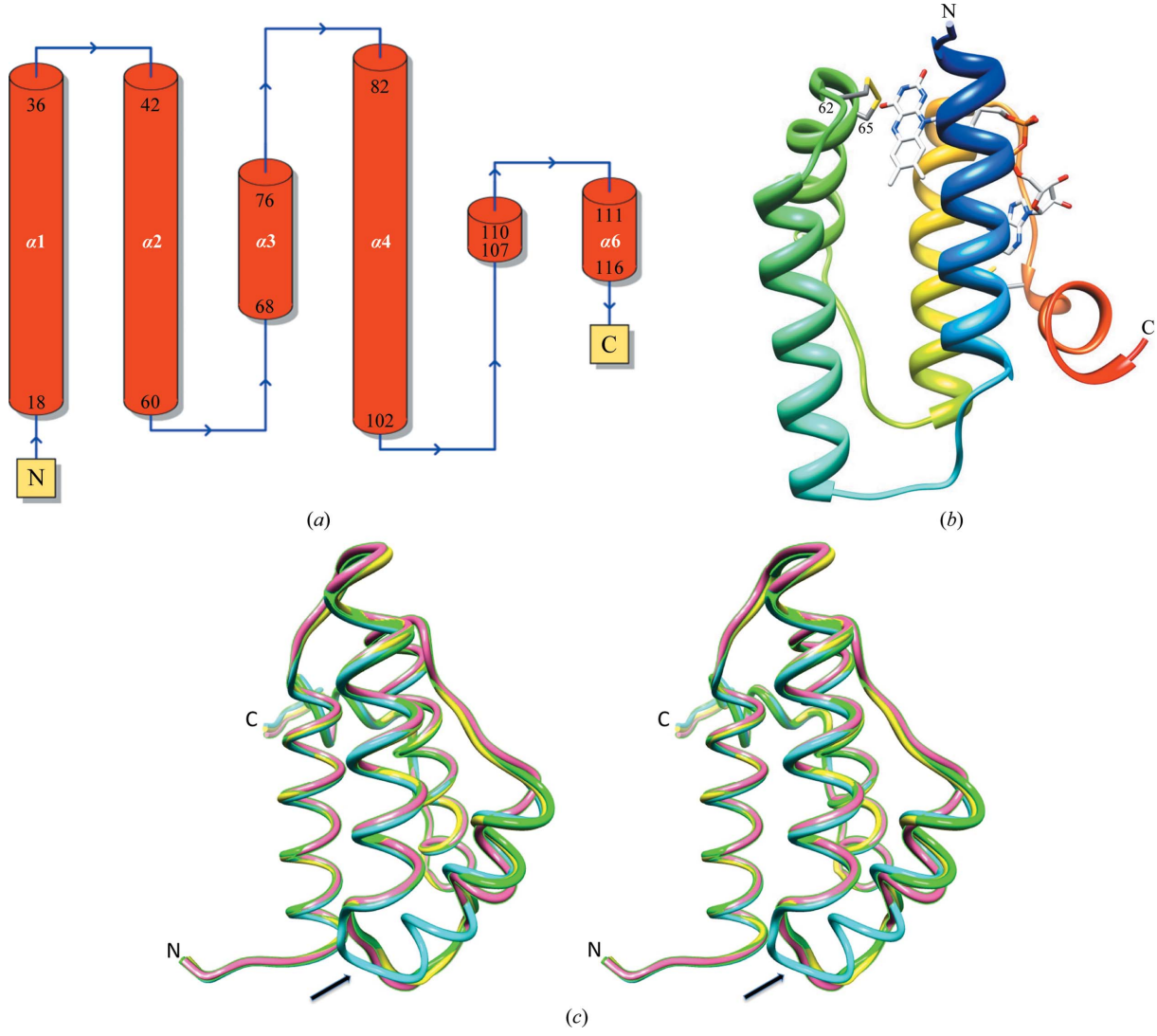

Figure 2
(*a*) A wiring diagram for the hsALR structure generated by *PROMOTIF* (Hutchinson & Thornton, 1996). The figure was adapted from *PDBSum* (Laskowski *et al.*, 2005). (*b*) A view of the hsALR monomer showing the bound FAD molecule and the Cys62–Cys65 disulfide bond, which are components of the putative catalytic site. The molecule is colored from blue to red to denote sequence position. (*c*) A cross-eyed stereo image of the overlap of the four protein monomers that comprise the crystallographic asymmetric unit. The chains are colored as follows: chain *A*, yellow; chain *B*, green; chain *C*, cyan; chain *D*, pink. The structural variability observed for the α2–α3 loop (residues 60–68) is highlighted by the arrow at the bottom right of the structure.

Table 1
Data-collection and refinement details.

Values in parentheses are for the outer shell.

Crystal	
Space group	$I4_1$
Unit-cell parameters (Å)	a = 99.68, c = 113.61
Data collection	
Source	Rigaku RUH2R
Detector	MAR 30 cm image plate
Wavelength (Å)	1.5418
Crystal-to-detector distance (mm)	175
2θ (°)	0.0
φ step (°)	1.0
No. of images	720
Collection strategy	Inverse beam [30° wedges]
Data processing	
Program	*HKL* v.1.9.1
Resolution (Å)	50–2.4
Completeness (%)	100 (100)
Multiplicity	30.88 [15.44 Bijvoets]
$R_{\rm merge}$	0.089 (0.345)
Refinement	
Program	*PHENIX* v.1.7_650
Resolution (Å)	19.64–2.40 (2.46–2.40)
Completeness (%)	98.3
$R_{\rm cryst}$	0.165 (0.191)
$R_{\rm free}$	0.212 (0.256)
R.m.s. deviations from ideality	
Bond lengths (Å)	0.007
Bond angles (°)	1.15
Ramachandran analysis	
Most favored (%)	91.8
All other allowed (%)	8.2
Outliers (%)	0
Final model	
Protein atoms	3642
Heterogen atoms	229
Solvent atoms	237
PDB code	3r7c

Table 2
Interface interactions.

(*a*) hsALR *AB* interface interactions. Interfaces were generated by *PISA* (Krissinel & Henrick, 2007).

Chain *A*	Distance (Å)	Chain *B*
Hydrogen bonds		
Asp48 OD1	2.94	Arg75 NH1
Gln51 OE1	2.46	Arg75 NH1
Gln51 OE1	3.58	Lys71 NZ
His54 NE2	2.68	Gln77 OE1
Arg75 NH2	3.37	Gln47 OE1
Arg75 NE	3.38	Gln47 OE1
Arg75 NH1	2.88	Gln51 OE1
Gln77 NE2	2.96	Pro78 O
Gln77 OE1	2.61	His54 NE2
Pro78 O	3.17	Gln77 NE2
Salt bridges		
Glu44 OE2	3.19	Arg75 NH2
Asp48 OD1	2.94	Arg75 NH1
Asp48 OD1	3.00	Arg75 NH2
His54 ND1	3.38	Asp74 OD1
Asp74 OD1	3.49	His54 ND1
Arg75 NH2	3.35	Glu44 OE1
Arg75 NH1	2.71	Asp48 OD1
Arg75 NH2	3.00	Asp48 OD1

(*b*) sALR *AB* interface interactions.

Chain *A*	Distance (Å)	Chain *B*
Hydrogen bonds		
Arg83 NH2	3.50	Gln47 OE1
Ser87 OG	3.50	Gln47 OE1
Ser87 OG	3.76	Gln47 NE2
Gln88 OE1	2.87	Gln47 NE2
Asp39 OD2	2.88	Gln51 NE2
Salt bridge		
Arg92 NH1	3.63	Glu44 O2

promote intermolecular interactions that facilitate molecular packing *via* coordination with the carboxylate groups of aspartic acid or glutamic acid residues that bridge the intermolecular interface (Trakhanov *et al.*, 1998; Zanotti *et al.*, 1998). In the $Cd_2Cl_4O_6$ cluster (Fig. 3*b*) Cd501 is coordinated by the carboxyl side chain of Asp74*A* of the *AC* dimer, three chloride ions (502, 503 and 504) and HOH506, while Cd500*A* is coordinated by the carboxyl side chain of Asp74*B* of the *BD* dimer, three chloride ions (502, 503 and 505) and HOH507, thus forming a bridge between the *AC* and *BD* dimers. The average bond lengths observed for atoms in the cluster are 2.61 Å for the Cd—Cl bonds, 2.46 Å for the Cd—O bonds and 3.82 Å for the Cd···Cd distance, which are in agreement with published data (Chen & Mak, 1991).

The dimer–dimer interface is also considerably larger (554 Å^2) than the interface (282 Å^2) observed in the native structure and involves more hydrogen bonds and salt-bridge interactions (see Table 2). Residues His54 and Lys58 have also undergone some rearrangement in the hsALR structure to accommodate the cluster, with His54 participating in both hydrogen and salt-bridge interaction at the dimer–dimer interface.

The other Cd clusters found on the surface of the protein include a CdO_5 cluster associated with Glu113*C*, a CdO_6 cluster associated with residues Glu44*C* and Gln47*C* and a CdO_5 cluster associated with residues Asp107*B* and Ser109*B*. However, these clusters are not involved in crystal-packing interactions.

3.3. Effect of the $Cd_2Cl_4O_6$ cluster on crystal packing

The orientation of the two dimers in the hsALR tetramer differs significantly from the orientation observed in the sALR tetramer. In the sALR tetramer the N- and C-terminal regions of the dimer face each other as illustrated in Fig. 3(*c*). It should be noted that residues 1–13 were not observed in either the sALR or hsALR structures and are randomly orientated in the interface. Thus, the addition of the 14-residue purification tag used in preparing the hsALR protein would further crowd the interface and could disrupt crystal-packing interactions. This crowding would explain why the hsALR protein failed to crystallize using the native sALR conditions and why the use of a similar 21-residue (MGHHHHHHHHHHSSGHIEGRH) construct failed to produce any crystals (Wu *et al.*, 2000). As illustrated in Fig. 3(*a*), the $Cd_2Cl_4O_6$ cluster anchors the dimers in a manner in which the N- and C-terminal regions of the each dimer face away from the dimer–dimer interface. This new tetramer organization better accommodates the addition of the bulky purification tag.

4. Conclusions

Here, we describe the structure determination of hsALR by Cd-SAD using a highly redundant data set collected on a home X-ray source and processed in 1998. The crystal structure revealed a tetramer composed of two hsALR dimers, which are bridged by a novel $Cd_2Cl_4O_6$ cluster *via* coordination of the side-chain O (OD1 and OD2) atoms of aspartic acid residues Asp74*A* and Asp74*B* located in the *AC* and *BD* dimers, respectively. The geometry of the $Cd_2Cl_4O_6$ cluster is similar to the structure reported by Chen & Mak (1991) of a dimeric diaquabis(betaine)tetrachlorodicadmium(II) complex (Cambridge Structural Database entry SIWSIA; Allen, 2002). A comparison of the native and His-tagged tetramers shows that the dimer–dimer interfaces are orientated 90° to each other. In the native sALR tetramer the two dimers associate such that the N- and C-terminal regions of the dimers are in close proximity, producing a crowded interface. In the hsALR tetramer the bridging $Cd_2Cl_4O_6$ cluster anchors the dimers in such a way that the N- and C-terminal regions of both dimers point away from the dimer–dimer interface. Thus, while the addition of the 14-residue purification tag could possibly disrupt the crowded dimer–dimer interface in the native sALR tetramer and affect crystal-packing interactions, it should have little impact on the hsALR dimer–dimer interface. The fact that no crystals were obtained for the His-tagged construct using native sALR crystallization conditions would tend to support this. In hindsight, removal of the purification tag may have been a good alternative since it would have avoided the crowding problems discussed above. However, the need to do this was eliminated by the determination of the sALR structure. The hsALR structure also provides a view of the dynamic nature of the $\alpha2$–$\alpha3$ loop and the putative catalytic site that may provide insight into substrate binding.

Finally, the success of the structure determination can be attributed to the improvements in structure-determination software and computer graphics that have been made over the past decade and highlights the value of retaining data and related files for future analysis and the need for archiving of the raw image data. We were fortunate in that the processed

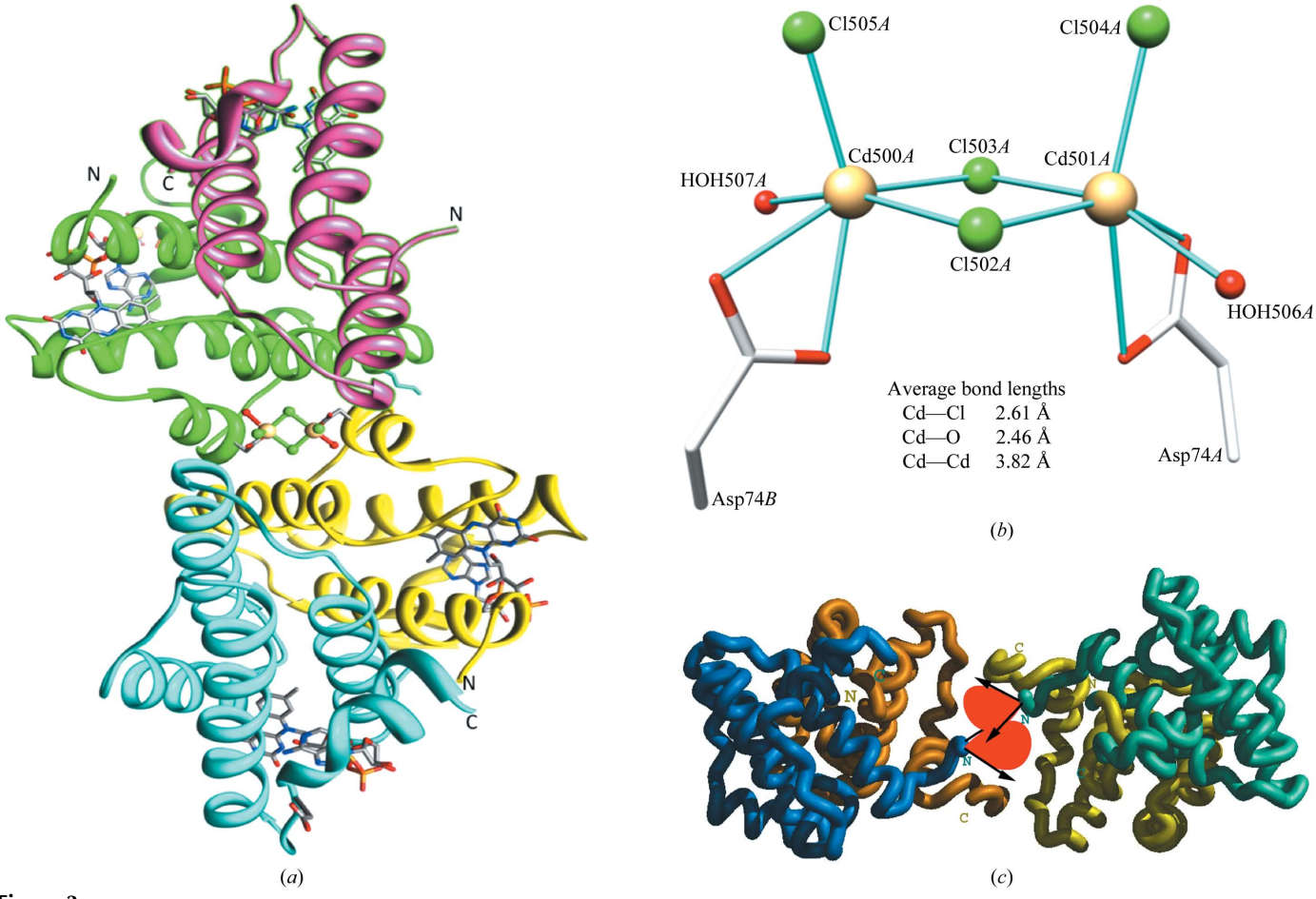

Figure 3
(*a*) A view of the hsALR tetramer showing local twofold symmetry and the bridging $Cd_2Cl_4O_6$ cluster. The *AC* and *BD* dimers are colored as follows: chain *A*, yellow; chain *B*, green; chain *C*, cyan; chain *D*, pink. Atoms making up the $Cd_2Cl_4O_6$ cluster are colored as follows: Cd, yellow; Cl, green; O, red; C, white. (*b*) A detailed view of the $Cd_2Cl_4O_6$ cluster. Here, each cadmium ion is hexadentate, coordinating three chloride ions, one water and two O atoms from Asp74. (*c*) A view of the sALR tetramer (PDB entry 1oqc). The sALR dimers are colored yellow and cyan, and tan and blue. Note that in the sALR tetramer the two dimers are positioned such that the N- and C-termini of two sALR molecules (one from each dimer) are pointing into the dimer–dimer interface. The addition of the 14-residue His tag (red cone) would disrupt the sALR dimer–dimer interface, leading to crystal-packing problems in the sALR crystal lattice and explains why no crystals of hsALR were produced using sALR crystallization protocols.

data were still available 12 years after data collection and that the preliminary work describing the experiment had been published. Unfortunately, the tape backup of the raw data proved to be unreadable, preventing the reprocessing of the data using current programs.

This work was supported in part by funds from the Georgia Research Alliance (BCW), University of Georgia startup funding (JPR) and the University of Georgia Research Foundation.

References

Adams, P. D. *et al.* (2010). *Acta Cryst.* D**66**, 213–221.
Adams, G. A., Maestri, M., Squiers, E. C., Alfrey, E. J., Starzl, T. E. & Dafoe, D. C. (1998). *Transplantation*, **65**, 32–36.
Allen, F. H. (2002). *Acta Cryst.* B**58**, 380–388.
Allen, S., Balabanidou, V., Sideris, D. P., Lisowsky, T. & Tokatlidis, K. (2005). *J. Mol. Biol.* **353**, 937–944.
Banci, L., Bertini, I., Calderone, V., Cefaro, C., Ciofi-Baffoni, S., Gallo, A., Kallergi, E., Lionaki, E., Pozidis, C. & Tokatlidis, K. (2011). *Proc. Natl Acad. Sci. USA*, **108**, 4811–4816.
Berman, H. M. *et al.* (2002). *Acta Cryst.* D**58**, 899–907.
Brünger, A. T. (1992). *Nature (London)*, **355**, 472–475.
Chen, X.-M. & Mak, T. C. W. (1991). *J. Chem. Crystallogr.* **21**, 27–32.
Emsley, P. & Cowtan, K. (2004). *Acta Cryst.* D**60**, 2126–2132.
Farrell, S. R. & Thorpe, C. (2005). *Biochemistry*, **44**, 1532–1541.
Francavilla, A., Ove, P., Polimeno, L., Coetzee, M., Makowka, L., Rose, J., Van Thiel, D. H. & Starzl, T. E. (1987). *Cancer Res.* **47**, 5600–5605.
Francavilla, A., Vujanovic, N. L., Polimeno, L., Azzarone, A., Iacobellis, A., Deleo, A., Hagiya, M., Whiteside, T. L. & Starzl, T. E. (1997). *Hepatology*, **25**, 411–415.
Gerhold, R. W., Lollis, L. A., McDougald, L. R. & Beckstead, R. B. (2011). *J. Parasitol.* **97**, 354–356.
Hutchinson, E. G. & Thornton, J. M. (1996). *Protein Sci.* **5**, 212–220.
Krissinel, E. & Henrick, K. (2007). *J. Mol. Biol.* **372**, 774–797.
Lange, H., Lisowsky, T., Gerber, J., Mühlenhoff, U., Kispal, G. & Lill, R. (2001). *EMBO Rep.* **2**, 715–720.
Laskowski, R. A., Chistyakov, V. V. & Thornton, J. M. (2005). *Nucleic Acids Res.* **33**, D266–D268.
Lisowsky, T. (1996). *Yeast*, **12**, 1501–1510.
Lisowsky, T., Lee, J. E., Polimeno, L., Francavilla, A. & Hofhaus, G. (2001). *Dig. Liver Dis.* **33**, 173–180.
Navaza, J. (2001). *Acta Cryst.* D**57**, 1367–1372.
Pettersen, E. F., Goddard, T. D., Huang, C. C., Couch, G. S., Greenblatt, D. M., Meng, E. C. & Ferrin, T. E. (2004). *J. Comput. Chem.* **25**, 1605–1612.
Polimeno, L., Capuano, F., Marangi, L. C., Margiotta, M., Lisowsky, T., Ierardi, E., Francavilla, R. & Francavilla, A. (2000). *Dig. Liver Dis.* **32**, 510–517.
Rose, J. P., Wu, C.-K., Dailey, T. A., Dailey, H. A. & Wang, B.-C. (1999). *Acta Cryst.* A**55**, C294.
Tanigawa, K., Sakaida, I., Masuhara, M., Hagiya, M. & Okita, K. (2000). *J. Gastroenterol.* **35**, 112–119.
Trakhanov, S., Kreimer, D. I., Parkin, S., Ames, G. F. & Rupp, B. (1998). *Protein Sci.* **7**, 600–604.
Wu, C.-K., Dailey, T. A., Dailey, H. A., Francavilla, A., Starzl, T. E., Wang, B.-C. & Rose, J. P. (2000). *Protein Pept. Lett.* **7**, 25–32.
Wu, C.-K., Dailey, T. A., Dailey, H. A., Wang, B.-C. & Rose, J. P. (2003). *Protein Sci.* **12**, 1109–1118.
Zanotti, G., Panzalorto, M., Marcato, A., Malpeli, G., Folli, C. & Berni, R. (1998). *Acta Cryst.* D**54**, 1049–1052.